ARMY RESEARCH LABORATORY

Guidance and Control of a Fin-Stabilized Projectile Based on Flight Dynamics with Reduced Sensor and Actuator Requirements

by Frank Fresconi

ARL-TR-5458 **February 2011**

Approved for public release; distribution unlimited.

NOTICES

Disclaimers

The findings in this report are not to be construed as an official Department of the Army position unless so designated by other authorized documents.

Citation of manufacturer's or trade names does not constitute an official endorsement or approval of the use thereof.

Destroy this report when it is no longer needed. Do not return it to the originator.

Army Research Laboratory
Aberdeen Proving Ground, MD 21005-5066

ARL-TR-5458 **February 2011**

Guidance and Control of a Fin-Stabilized Projectile Based on Flight Dynamics with Reduced Sensor and Actuator Requirements

Frank Fresconi
Weapons and Materials Research Directorate, ARL

Approved for public release; distribution unlimited.

REPORT DOCUMENTATION PAGE	Form Approved OMB No. 0704-0188

Public reporting burden for this collection of information is estimated to average 1 hour per response, including the time for reviewing instructions, searching existing data sources, gathering and maintaining the data needed, and completing and reviewing the collection information. Send comments regarding this burden estimate or any other aspect of this collection of information, including suggestions for reducing the burden, to Department of Defense, Washington Headquarters Services, Directorate for Information Operations and Reports (0704-0188), 1215 Jefferson Davis Highway, Suite 1204, Arlington, VA 22202-4302. Respondents should be aware that notwithstanding any other provision of law, no person shall be subject to any penalty for failing to comply with a collection of information if it does not display a currently valid OMB control number.
PLEASE DO NOT RETURN YOUR FORM TO THE ABOVE ADDRESS.

1. REPORT DATE *(DD-MM-YYYY)*	2. REPORT TYPE	3. DATES COVERED (From - To)
February 2011	Final	January 2008–October 2010

4. TITLE AND SUBTITLE
Guidance and Control of a Fin-Stabilized Projectile Based on Flight Dynamics with Reduced Sensor and Actuator Requirements

5a. CONTRACT NUMBER

5b. GRANT NUMBER

5c. PROGRAM ELEMENT NUMBER

6. AUTHOR(S)
Frank Fresconi

5d. PROJECT NUMBER
AH43

5e. TASK NUMBER

5f. WORK UNIT NUMBER

7. PERFORMING ORGANIZATION NAME(S) AND ADDRESS(ES)
U.S. Army Research Laboratory
ATTN: RDRL-WML-E
Aberdeen Proving Ground, MD 21005-5066

8. PERFORMING ORGANIZATION REPORT NUMBER
ARL-TR-5458

9. SPONSORING/MONITORING AGENCY NAME(S) AND ADDRESS(ES)

10. SPONSOR/MONITOR'S ACRONYM(S)

11. SPONSOR/MONITOR'S REPORT NUMBER(S)

12. DISTRIBUTION/AVAILABILITY STATEMENT
Approved for public release; distribution unlimited.

13. SUPPLEMENTARY NOTES

14. ABSTRACT
Successfully guiding a projectile launched from a gun is an extremely challenging task. Striking a balance between performance and affordability requires innovative solutions. This effort introduces a unique guidance and control strategy, which enables precision and trajectory shaping with reduced sensor and actuator needs. The derivation of this guidance and control algorithm is based on flight dynamics. Flight experiments were conducted to verify that the algorithm guided the projectile to the target and demonstrate rapid application to different airframes. Features of the algorithm, such as expected precision, maneuver conservation, and trajectory shaping, were investigated through modeling and simulation. Position bias errors drove the precision; errors due to the guidance and control algorithm were on the order of 0.1 m. An analysis was conducted on the lateral acceleration available from the airframe, lateral acceleration required for this algorithm, and lateral acceleration required for classic proportional navigation. For control authority-limited munitions, proportional navigation was unable to intercept the target point while the current guidance algorithm successfully hit the target. Steepening the angle-of-fall to vertical is possible with this algorithm provided the airframe possesses the necessary maneuverability.

15. SUBJECT TERMS
Precision projectile, guidance, navigation, and flight control, algorithm

16. SECURITY CLASSIFICATION OF:			17. LIMITATION OF ABSTRACT	18. NUMBER OF PAGES	19a. NAME OF RESPONSIBLE PERSON
a. REPORT	b. ABSTRACT	c. THIS PAGE			Frank Fresconi
Unclassified	Unclassified	Unclassified	UU	38	19b. TELEPHONE NUMBER (*Include area code*) (410) 306-0794

Standard Form 298 (Rev. 8/98)
Prescribed by ANSI Std. Z39.18

Contents

List of Figures

List of Tables

1. Introduction

This effort is motivated by the need for affordable precision fires with timely lethality and low collateral damage. This need is especially urgent for indirect fire since range and angle-of-fall characteristics of these munitions are attractive in current conflicts. Programs have addressed precision munitions (*1–4*). These solutions have not attained widespread usage, however, due to factors such as excess technical complexity, individual unit production cost, overall program cost, limited performance, and difficulties associated with employing the technology on the battlefield.

A variety of technical challenges are posed during the development of gun-launched precision munitions. The shock and vibration encountered during the gun launch event impart thousands of time the force of gravity in vastly different frequency regimes on mechanical and electrical components. Gun rifling gyroscopically stabilizes the projectile in flight, which results in unique, complex flight dynamics. Constraints on handling, loading, tube launch, and system trades severely limit the space available for guidance components such as sensors, processors, and actuators.

Further challenges in the guidance, navigation, and control (GNC) for precision munitions include the balance of affordability with performance. A full suite of high-fidelity sensors and associated algorithms to provide estimates of all projectile and target states in flight is not fiscally feasible for a gun-launched application. Likewise, the maneuver system complexity must be minimized. A generalized GNC solution with minimal tailoring for different calibers enables rapid application of the technology with reduced aerodynamic characterization and time-consuming gain scheduling. Achieving these affordability goals while still meeting performance objectives is a nontrivial task.

A simple, elegant solution to the affordable precision munition problem is offered in this effort. This system uses a single-axis control actuation system (CAS) with canards on a rolling fin-stabilized airframe. Emplacing the control mechanism at the nose of a fin-stabilized projectile provides the maximum control authority (*5*, *6*), which reduces the actuator burden. A global positioning system (GPS) receiver with upfinding provides information concerning the projectile state. The airframe development is essential to this concept. The roll rate of the projectile must meet CAS and GPS requirements. The control authority must be sufficient to remove ballistic dispersion errors and also provide range extension and trajectory shaping to steepen angle-of-fall. Furthermore, the statically stable airframe must be dynamically stable during flight since costly feedback sensors are not used for active damping. Dynamic stability may be inferred through characterizing the aerodynamics (*7–9*). This precision munition solution is enabled by a novel guidance and control scheme, which is the focus of this work.

Guidance and control of projectiles has been explored in the literature (*1*, *10–21*). The concepts detailed in these papers include direct and indirect fire fin-stabilized and spin-stabilized projectiles with control mechanisms such as pulsed jets, canards, fins, and ram air. These guidance and control strategies can be loosely broken into approaches which track the state of the projectile near the current time (*11*, *12*) and those which forecast the state of the projectile near the target (*13–19*).

When precision munitions feature low control authority, the guidance system is often used simply to remove uncompensated error sources such as atmospheric effects, muzzle velocity variations, etc. In keeping with this approach, the guidance and control can be loaded with nominal trajectory information prior to launch. The goal of the flight controller at a given time becomes removing the difference between the appropriate projectile states with the nominal states. This technique has been explored by Jitpraphai and Costello (*11*) and Rogers and Costello (*12*).

Impact point prediction is an attractive option in some situations. In this guidance scheme, the specific trajectory taken to remove miss distance is not as important as it is in the trajectory tracking approach. This is an important feature since over-control of control authority-limited precision munitions may occur when trajectory tracking algorithms are not properly constructed. Impact point prediction algorithms contain a dynamic model of projectile flight. This model is used to estimate the impact point of the projectile. The geometry of the miss distance forms a feedback loop to remove error between target and projectile impact. The control effort is often minimized since the physics of flight are built into impact point prediction. This guidance law has been shown to be a special form of traditional proportional navigation where the zero-effort miss and time-to-go are based on the impact point prediction (*13*). Linear (*13*, *16*, *17*) and nonlinear (*14*, *15*, *18*, *19*) control techniques have been applied to the impact point prediction guidance approach. Furthermore, states other than position, such as impact angle, may also be controlled at impact (*17*, *20*).

The present work makes a few contributions to the literature. The flight dynamic model used in the impact point prediction includes the control mechanism that permits novel trajectory shaping. A new flight control law is developed that enables high precision and minimal tuning for a given airframe. Importantly, projectile states input to the flight dynamic model were obtainable from affordable, real-world devices. A balance was struck between dynamic model fidelity and the practical realities of data availability in flight. This algorithm reduced the control effort by building the ballistic flight (and, therefore, minimal energy) into the guidance scheme. Real-time implementation of the algorithm for flight experiments was facilitated by a closed-form solution to the flight dynamic equations. Lastly, the application of this guidance and control algorithm for the precision munition solution outlined previously and demonstration in end-to-end guided flight experiments validates these technologies.

This report is organized as follows: derivation of the guidance and flight control algorithm, experimental verification of the guidance and control during successful guide-to-hit flights, six degree-of-freedom (6-DOF) modeling and Monte Carlo system simulations demonstrating key features of the guidance and control such as precision, conservation of maneuvers, and trajectory shaping, and finally, experimental support for the rapid adaptability of the approach to different airframes.

2. Guidance and Flight Control Algorithm

A block diagram of the guidance and flight control algorithm is provided in figure 1. The algorithm requires a few different types of input. Prior to each flight, the Earth-centered, Earth-fixed (ECEF) coordinates of the gun ($\vec{x}_G^{ECEF}$), target ($\vec{x}_T^{ECEF}$), and time in flight to begin guidance (t_{guide}) were loaded into the algorithm. Estimates of the inertial position ($\vec{x}^{ECEF}$) and velocity ($\dot{\vec{x}}^{ECEF}$) in ECEF coordinates of the projectile are provided by a GPS receiver in flight, typically at a rate of 1–5 Hz. The GPS also outputs a discrete pulse (denoted as up-pulse) when the GPS antenna is oriented up (i.e., perpendicular to the ground and toward the sky), which is interrogated to obtain roll orientation and roll rate.

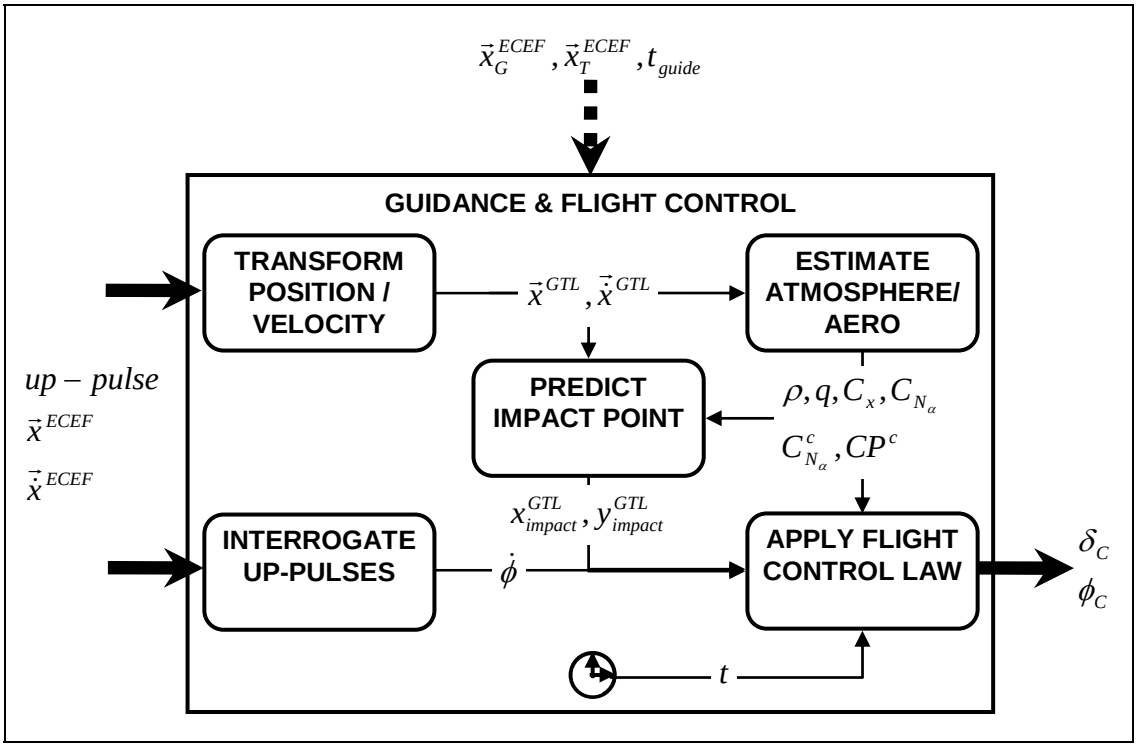

Figure 1. Guidance and control algorithm block diagram.

These data (gun location, target location, guidance start time, up-pulse, projectile position, and projectile velocity) are used in the algorithm to compute the guidance commands: canard amplitude (δ_c) and phase angle (ϕ_c). Recall the system concept for this effort. The canards oscillate to positive and negative deflection angles in sync with the roll orientation of the projectile. A reference sinusoid signal is formed based on information from the GPS and guidance and flight control algorithm for the canards to track. The GPS up-pulse provides the zero roll orientation and period of the sinusoid. The amplitude of the sinusoid and phasing with respect to the zero roll orientation are given by the guidance and flight control algorithm. Essentially, the magnitude of the maneuver is provided by the canard amplitude and the direction of the maneuver is given by the canard phase angle. This reference sinusoid is tracked by the maneuver system. For more description of this precision munition system, see Fresconi et al. (*22*).

The details within the guidance and flight control block of figure 1 are the topic of this effort. While GPS data are in the ECEF frame the impact point prediction takes place in a local tangent plane frame, denoted as the gun-target line (GTL) frame. The origin of this frame is at the gun and the *x*-axis (referred to as downrange) runs through the target. The *z*-axis (denoted as altitude) points down and the *y*-axis (referred to as crossrange) completes a right-handed coordinate system. The transformation of position from the ECEF to GTL frame is given below:

$$\begin{bmatrix} x^{GTL} \\ y^{GTL} \\ z^{GTL} \end{bmatrix} = \begin{bmatrix} \cos\gamma & \sin\gamma & 0 \\ -\sin\gamma & \cos\gamma & 0 \\ 0 & 0 & 1 \end{bmatrix} \begin{bmatrix} -\sin\theta_{ref}^{lat}\cos\theta_{ref}^{long} & -\sin\theta_{ref}^{lat}\sin\theta_{ref}^{long} & \cos\theta_{ref}^{lat} \\ -\sin\theta_{ref}^{long} & \cos\theta_{ref}^{long} & 0 \\ -\cos\theta_{ref}^{lat}\cos\theta_{ref}^{long} & -\cos\theta_{ref}^{lat}\sin\theta_{ref}^{long} & -\sin\theta_{ref}^{lat} \end{bmatrix} \begin{bmatrix} x^{ECEF} - x_{ref}^{ECEF} \\ y^{ECEF} - y_{ref}^{ECEF} \\ z^{ECEF} - z_{ref}^{ECEF} \end{bmatrix} \quad (1)$$

Here, $[x^{GTL}, y^{GTL}, z^{GTL}]$ are the GTL coordinates of position, γ is the angle in the horizontal plane between the north and GTL *x*-axis, θ_{ref}^{lat} is the latitude of a reference position, θ_{ref}^{long} is the longitude of a reference position, $[x^{ECEF}, y^{ECEF}, z^{ECEF}]$ are the ECEF coordinates of position, and $[x_{ref}^{ECEF}, y_{ref}^{ECEF}, z_{ref}^{ECEF}]$ are the ECEF coordinates of a reference position. The gun location was used as the reference position.

The angle γ is calculated using the ECEF coordinates of the target $[x_T^{ECEF}, y_T^{ECEF}, z_T^{ECEF}]$ and gun position by using the following two equations.

$$\begin{bmatrix} x^{NED} \\ y^{NED} \\ z^{NED} \end{bmatrix} = \begin{bmatrix} -\sin\theta_{ref}^{lat}\cos\theta_{ref}^{long} & -\sin\theta_{ref}^{lat}\sin\theta_{ref}^{long} & \cos\theta_{ref}^{lat} \\ -\sin\theta_{ref}^{long} & \cos\theta_{ref}^{long} & 0 \\ -\cos\theta_{ref}^{lat}\cos\theta_{ref}^{long} & -\cos\theta_{ref}^{lat}\sin\theta_{ref}^{long} & -\sin\theta_{ref}^{lat} \end{bmatrix} \begin{bmatrix} x_T^{ECEF} - x_G^{ECEF} \\ y_T^{ECEF} - y_G^{ECEF} \\ z_T^{ECEF} - z_G^{ECEF} \end{bmatrix} \quad (2)$$

$$\gamma = \arctan\left[\frac{y^{NED}}{x^{NED}}\right] \tag{3}$$

The transformation of velocity from ECEF to GTL differs from equation 1 in that it is unnecessary to subtract a reference position.

Atmospheric and aerodynamic data are necessary to run the dynamic model for the impact point prediction. The 1976 U.S. Standard Atmosphere is built into the algorithm. The GTL *z*-coordinate is used to estimate altitude about sea level. Altitude and GPS-derived total velocity are used in the standard atmosphere model to estimate atmospheric density, speed of sound, Mach number, and dynamic pressure. It is significant that there is no need for added complexity and cost of providing a meteorological update to the algorithm prior to firing for better estimating atmospheric and flight conditions. Aerodynamic coefficients for axial force (C_x), normal force of the body (C_{N_α}), normal force of the canards ($C^c_{N_\alpha}$), and center-of-pressure of the canards (CP^c) are interpolated based on the Mach number.

Atmospheric density (ρ), dynamic pressure (q), aerodynamic coefficients, and GTL position ($\vec{x}^{GTL}$) and velocity ($\dot{\vec{x}}^{GTL}$) are input to the flight dynamic model for impact point prediction. A point-mass model with normal force of the body and control mechanism is the flight dynamic model used in this effort. Adding the normal force to the model enables the maneuvers of the airframe to be included in the guidance scheme. The modeling errors for point mass are small, even when compared with the 6-DOF (*22*). Moreover, this model does not need projectile states such as angle-of-attack, which are difficult and costly to obtain on a gun-launched airframe. Sensor requirements are reduced because only the GPS is necessary.

The governing equations for the point mass model with normal force of the body and control mechanism are provided:

$$\begin{aligned}
\ddot{x} &= \frac{-\pi C_x D^2 \rho V}{8m}\dot{x} + \left(\cos(\phi_c)\cos(\psi)\sin(\theta) + \sin(\phi_c)\sin(\psi)\right)\frac{\left(F_N^b + F_N^c\right)}{m} \\
\ddot{y} &= \frac{-\pi C_x D^2 \rho V}{8m}\dot{y} + \left(\cos(\phi_c)\sin(\psi)\sin(\theta) - \sin(\phi_c)\cos(\psi)\right)\frac{\left(F_N^b + F_N^c\right)}{m} \\
\ddot{z} &= \frac{-\pi C_x D^2 \rho V}{8m}\dot{z} + g + \left(\cos(\phi_c)\cos(\theta)\right)\frac{\left(F_N^b + F_N^c\right)}{m}
\end{aligned} \tag{4}$$

The mass (m) and diameter (D) of the projectile is required for the calculations. Total velocity of the projectile (V) was estimated from the GPS. Maneuver direction is supplied by the guidance command, ϕ_c. The angles for pitch (θ) and yaw (ψ) of the airframe with respect to the Earth frame are obtained from the GPS velocity vector assuming small angle-of-attack.

$$\theta = \arctan\left[\frac{-\dot{z}}{\sqrt{\dot{y}^2 + \dot{x}^2}}\right] \tag{5}$$

$$\psi = \arctan\left[\frac{\dot{y}}{\dot{x}}\right] \tag{6}$$

Normal force of the body (F_N^b) was assessed using the standard relation,

$$F_N^b = qSC_{N_\alpha}\overline{\alpha}\,, \tag{7}$$

where $S = \pi/4\,D^2$ is the aerodynamic reference area, and $\overline{\alpha}$ is the average total angle-of-attack.

An equation was derived for the normal force of the control mechanism (F_N^c) by averaging over a roll cycle since the airframe was rolling. This equation takes the following form:

$$F_N^c = \frac{2}{\pi}\int_0^\pi qSC_{N_\alpha}^c(\alpha+\delta)d\phi = \frac{2}{\pi}\int_0^\pi qSC_{N_\alpha}^c[\alpha+\delta_c\sin(\phi)]d\phi = qSC_{N_\alpha}^c\left(\overline{\alpha}+\frac{4}{\pi}\delta_c\right). \tag{8}$$

Here, α is the instantaneous total angle-of-attack. The known sinusoidal function for canard deflection with roll angle is used in this relation ($\delta = \delta_c\sin(\phi+\phi_c)$).

The nonlinear, coupled, ordinary differential equations in equation 4 were solved analytically using symbolic math tools. This closed-form solution was used in an iterative method, Newton-Raphson, to determine the time of impact. Essentially, the equation for the *z*-direction position and *z*-direction velocity are used to determine the time from launch until the projectile passes through the *z*-coordinate of the target. This equation takes the form,

$$t_{impact}^{new} = t_{impact}^{old} - \frac{-(z_T^{GTL} + z_{impact}^{GTL})}{\dot{z}_{impact}^{GTL}}. \tag{9}$$

The iterative nonlinear solver was run until the residual between successive estimates of the time of impact fell below a threshold of 0.001 s. This time of flight from launch to impact is used in the closed-form solution for the *x* and *y* position to obtain the downrange and crossrange impact point. A by-product of these calculations, not explicitly used in the algorithm, is the time-to-go until impact.

The roll rate is used in the endgame flight control law; therefore, the time between GPS up-pulses is clocked to estimate the roll period. This calculation is simply inverted to obtain roll rate.

The flight control law is broken into three stages: ballistic, glide, and endgame. No maneuvers are performed during the ballistic phase. The optimal time to begin maneuvers for maximum control authority is dependent on the nonlinear dynamics of the airframe and varies with parameters such as quadrant elevation. A decent rule-of-thumb for optimal maneuver time of canard-controlled fin-stabilized projectiles, based on numerous flight dynamic characterizations (*24*), is to begin maneuvers near apogee. An onboard clock supplies time since launch to transition to the glide phase.

The goal of the glide stage of guidance is to extend range and enable trajectory shaping by steepening the angle-of-fall. One aspect of the glide flight controller is to remove projectile drift. Drift is a flight dynamic phenomenon, which occurs due to an interaction of gravity, aerodynamic pitching moment, and projectile spin (*7*). Drift must be removed in rolling airframes to maximize range otherwise energy will be spent in unnecessarily increasing the crossrange position. The flight controller providing the guidance commands during the glide phase takes the following form:

$$\phi_c = \arctan\left[\frac{K_{PG}\left(y^{GTL} - y_T^{GTL}\right) + K_{DG}\left(\dot{y}^{GTL} - \dot{y}_T^{GTL}\right)}{-\left(z^{GTL} - z_T^{GTL}\right)}\right] \tag{10}$$

$$\delta_c = \delta_{MAX} \tag{11}$$

In these expressions, K_{PG} is the glide proportional gain, K_{DG} is the glide derivative gain, and δ_{MAX} is the maximum canard amplitude. The maneuver direction controller seeks to remove error in crossrange position and get the inertial velocity vector pointed along the downrange axis. Studies have optimized this glide controller for rolling projectiles (*24*). The maneuver magnitude is saturated since the intent of the glide phase is to maximize maneuverability.

Impact point predictions are performed during the glide phase to determine the transition point into the endgame guidance. When the root-sum-squared distance in the ground plane from the predicted impact point to the gun exceeds the downrange distance of the target, then the endgame phase begins.

Trajectory shaping was achieved though a trajectory shaping parameter (the angle-of-attack $\overline{\alpha}$). A glide-induced angle-of-attack was entered into the flight dynamic model along with a maneuver direction (ϕ_c) to pitch the airframe over. Essentially, the impact point prediction was executed as if the projectile were to perform a down maneuver for the entire flight. This feature delays the transition from glide to endgame since the predicted impact with the down maneuver is shorter than the ballistic impact. The end result is a steeper angle-of-fall because the projectile glides for longer before pitching over. High confidence in the delayed transition point is ensured since the flight physics are built into the algorithm.

The objective of the endgame stage is to minimize miss distance. Here, the task is to find a suitable relationship between canard deflection and miss distance since the maneuver magnitude must scale with miss distance. As with the impact point prediction, the approach taken was to build the flight dynamics into the endgame maneuver magnitude controller to enable a generalized, physics-based solution.

A simplified, steady-state condition for the airframe, the equations for the normal force of the body and control mechanism are combined to write the total normal force (F_N) acting on the projectile as

$$F_N = F_N^b + F_N^c = qSC_{N_\alpha}\overline{\alpha} + \frac{4}{\pi}qSC_{N_\alpha}^c\left(\overline{\alpha} + \delta_c\right). \tag{12}$$

The average angle-of-attack of the projectile is near zero during the endgame since the airframe is making minor corrections in all directions to remove miss distance. The only normal force acting on the body at endgame is due to the control normal force. Control force acts at the center-of-pressure of the control mechanism and forms a moment about the center-of-gravity of the airframe (CG), permitting the control moment (M^c) to be calculated:

$$M^c = \frac{4}{\pi}qSC_{N\alpha}^c\delta_c(CP^c - CG). \tag{13}$$

This expression for control moment during endgame is used in a governing equation for rotational dynamics.

$$M^c = I_{trans}\dot{\omega}. \tag{14}$$

Transverse inertia of the airframe is I_{trans} and $\dot{\omega}$ is the rotational acceleration of the body. This equation assumes an inertial reference frame is fixed to the airframe. This is usually a poor assumption; however, the nature of feedback control relaxes this condition. The angular acceleration of the airframe is expressed as a double derivative of angle ($\ddot{\lambda}$) using the definition of angular velocity. The rotational acceleration is re-cast as

$$\dot{\omega} = \ddot{\lambda}. \tag{15}$$

Now, the scales for the angle and time in the angular acceleration term are defined.

$$d\lambda \sim e_\lambda \tag{16}$$

$$dt \sim 1/\dot{\phi} \tag{17}$$

These scales are chosen because the controller seeks to remove the angular error between the target and the predicted impact point over a roll cycle. The angular error was calculated in the plane normal to the line of sight from the airframe to the target. The equation for the angular error was obtained from trigonometry:

$$e_\lambda = \arctan\left\{\frac{\left[\frac{-\left(z^{GTL}-z_T^{GTL}\right)\sqrt{\left(x_{impact}^{GTL}-x_T^{GTL}\right)^2+\left(y_{impact}^{GTL}-y_T^{GTL}\right)^2}}{\sqrt{\left(x^{GTL}-x_{impact}^{GTL}\right)^2+\left(y^{GTL}-y_{impact}^{GTL}\right)^2+\left(z^{GTL}-z_{impact}^{GTL}\right)^2}}\right]}{\sqrt{\left(x^{GTL}-x_T^{GTL}\right)^2+\left(y^{GTL}-y_T^{GTL}\right)^2+\left(z^{GTL}-z_T^{GTL}\right)^2}}\right\} \tag{18}$$

All information required to relate canard deflection to impact error is now assembled. The final relationship for canard deflection during the endgame is provided below. A proportional gain (K_{PE}) is added to take up any error in the dynamic modeling:

$$\delta_c = K_{PE}\frac{\pi I_{trans} e_\lambda \dot{\phi}^2}{4qSC_{N\alpha}^c(CP^c - CG)}. \tag{19}$$

Qualitatively, this expression is attractive since the canard deflection scales proportionally with angular error, transverse inertia and roll rate (e.g., the larger the angular error the larger the canard deflection) and inversely proportional to the control moment (e.g., the larger the control moment the smaller the canard deflection). Building the flight dynamics into the flight control enables rapid applicability (less aerodynamic characterization, less gain scheduling) to different applications.

The errors in crossrange and downrange position provide the maneuver direction:

$$\phi_c = \arctan\left[\frac{\left(y_{impact}^{GTL}-y_T^{GTL}\right)}{-\left(x_{impact}^{GTL}-x_T^{GTL}\right)}\right]. \tag{20}$$

Stability analysis was not conducted on this control algorithm due to the system complexity. Rather, closed-loop Monte Carlo simulations are presented in section 3.

3. Experimental Verification During Guided Flights

Flight experiments were performed with the guidance and control algorithm outlined previously. Auto-code generation tools were used to facilitate embedding the algorithms on a digital signal processor (DSP) for real-time processing during flight. A 20-Hz update rate was used for the guidance and control algorithm during the experiments. Throughput demand of the algorithm at

this rate was low on the DSP due to the closed form solution technique detailed previously. A series of laboratory experiments were performed to verify algorithm implementation prior to flight.

A 155-mm fin-stabilized projectile was fired during these experiments. This projectile was equipped with the maneuver system and GPS in accordance with the concept previously discussed. A custom-built instrumentation package, containing magnetometers, accelerometers, gyroscopes, solar sensors, and a telemetry system, were included in the projectile for diagnostic purposes. Telemetry was used to obtain guidance and control algorithm input and calculations (shown in figures 2–7 and figure 13) during flight.

The experiments were conducted at the Yuma Proving Ground, AZ. Full-spectrum ballistic range instrumentation, including high-speed cameras, flight-tracking cameras, tracking radar, and telemetry receivers, was used. Projectiles were launched at approximately 696 m/s muzzle velocity at a 50° quadrant elevation. A target was placed 16,420 m from the gun. The ECEF coordinates of the gun and target, as well as the guidance start time of 25 s, were input to the algorithm before loading the projectile into the gun.

An example of the GPS data input to the guidance and control algorithm is presented in figures 2–4. Projectile position data are given in figure 2. The target position is at 16420 m downrange, 0 m crossrange, and 0 m altitude in these plots. The projectile flew over 15 km downrange and reached a maximum altitude over 6 km. Crossrange position data illustrated the efficacy of the guidance commands. The projectile drifted over 30 m off the gun-target line before course correcting to the target.

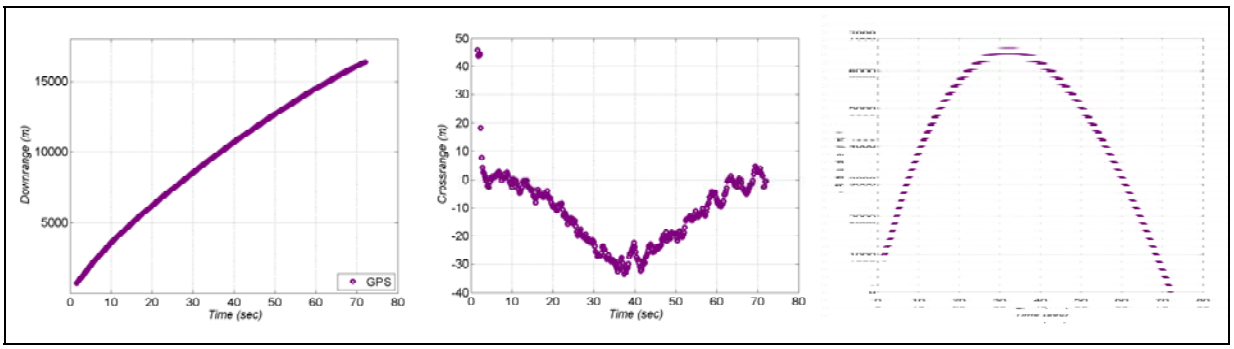

Figure 2. Position from GPS during the flight experiments.

The velocity data contained in figure 3 are expressed in a line-of-fire (LOF) coordinate system where the *x*-axis is along the LOF of the gun. The *y*-axis is in the horizontal plane and to the right when viewed from behind the gun and the *z*-axis completes a right-hand system. Velocity decay and overturning are evident in the *x*-axis and *z*-axis velocity, respectively. Typical spread in the velocity data is apparent in the *y*-axis velocity due to the small scale.

Roll rate of the projectile needed for the guidance and control algorithm is shown in figure 4. An approximate 300% change in roll rate was seen with some relatively large roll rate changes within the first 20 s of flight.

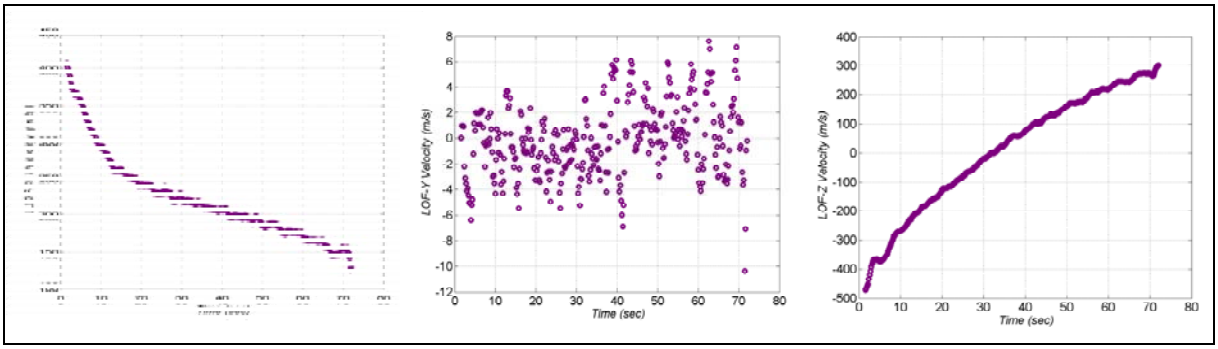

Figure 3. Velocity from GPS during the flight experiments.

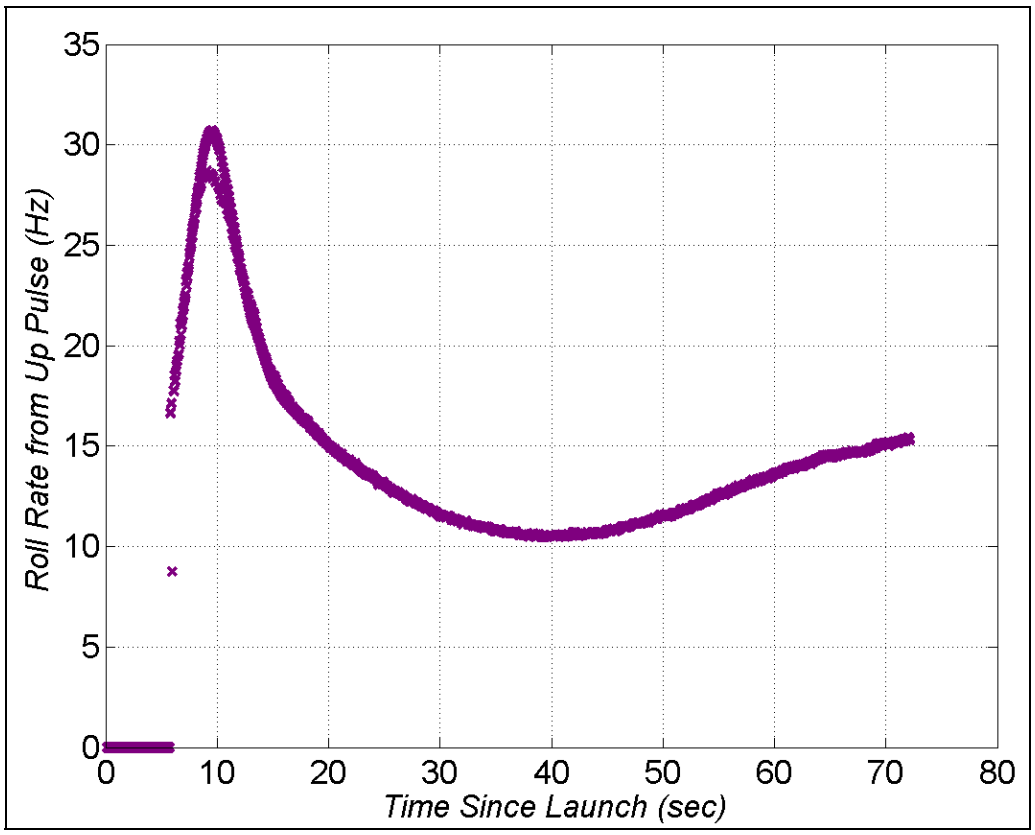

Figure 4. Roll rate from GPS upfinding during the flight experiments.

GPS data were used along with preliminary calculations, which estimated the atmospheric density, dynamic pressure, and aerodynamic coefficients to predict impact point. Downrange and crossrange impact point predictions during flight are presented in figure 5. The number of iterations required for the nonlinear solver to converge was between four (farther from impact during flight) and one (closer to impact during flight). The glide phase in the flight controller

was quickly passed through since the geometry of this engagement did not warrant glide. A value of K_{PE} = 5 was used for the endgame proportional gain.

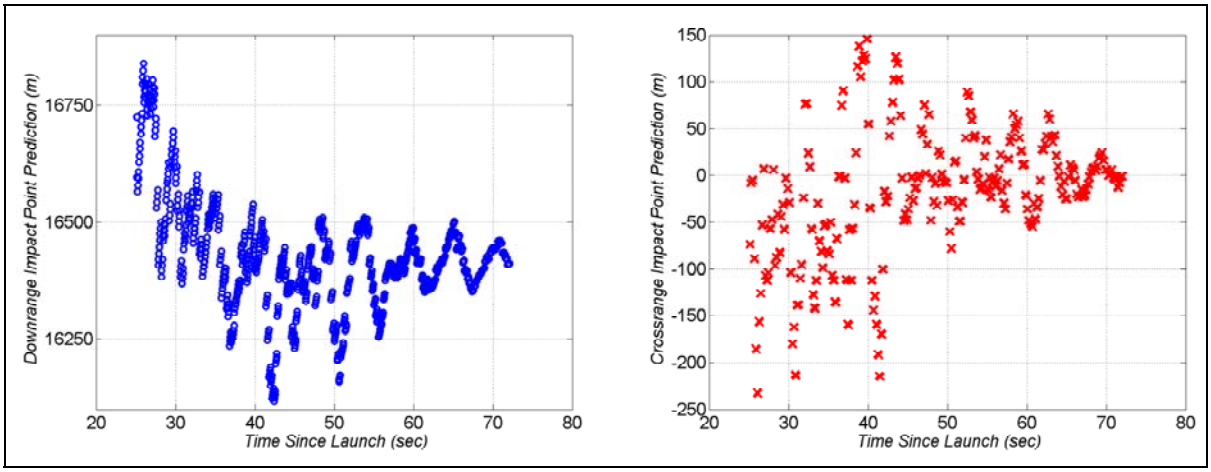

Figure 5. Downrange and crossrange impact point prediction guidance during the flight experiments.

The target was located at 16,420 m downrange and 0 m crossrange. The data in figure 5 portrays, for example, that at 60 s into flight the algorithm is predicting a downrange impact near 16,500 m and crossrange impact 50 m to the left (when viewed from behind the gun). Impact prediction fluctuated early in flight before converging to the target point. Three effects contribute to this variation: error in the flight dynamic model (likely not significant as shown in Fresconi et al. [*23*]), error in the input to the dynamic model (likely significant, especially GPS data), and uncertainty concerning unknown atmospheric conditions (e.g., wind, density) that the projectile has yet to fly through (likely significant). Despite these fluctuations, the impact point prediction algorithm and guided airframe converge on the target point.

The data in figure 5 suggest that the projectile was initially flying long and to the left of the target before correcting course. These findings are supported by the GPS position data.

A snapshot of a few samples of the impact point predictions and associated maneuver direction during endgame are given in figure 6 to elucidate the coupling between the flight dynamic modeling and guidance commands. Data in figure 6a were obtained by subtracting the predicted downrange and crossrange impact point from the target point. During this snapshot, the projectile was forecast to fall short (by 45 m to 70 m) and to the left (by 0 m to 25 m) of the target. Maneuvers were commanded up and slightly to the right to remove this miss geometry as shown in the illustration of figure 6b.

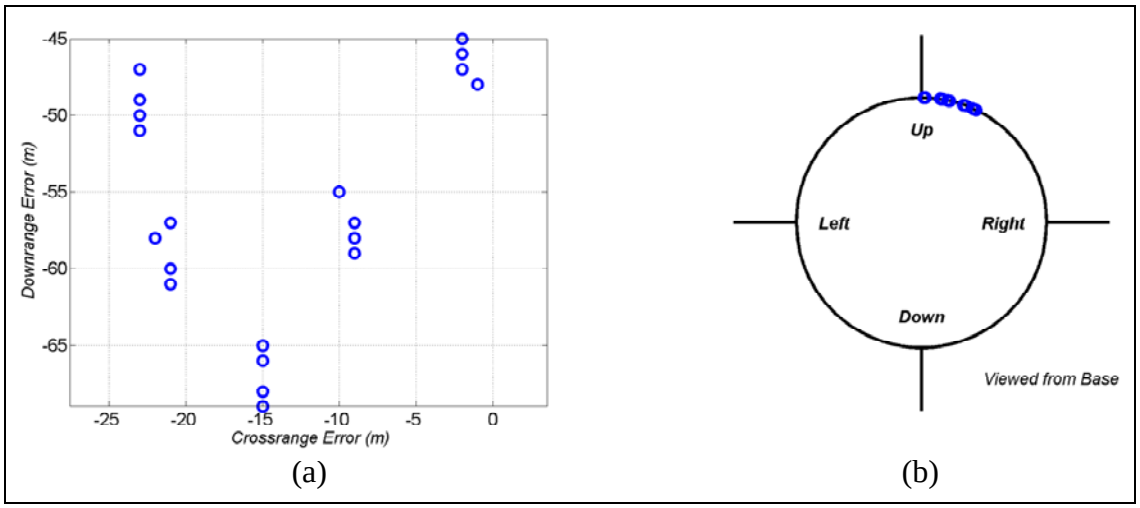

Figure 6. Visualization of impact point prediction-to-target location error (a) and resulting guidance canard phase angle command (b) during the flight experiments.

Guidance commands throughout the entire experimental flight are provided in figure 7. Canard amplitude varies from minimum to maximum based on input to equation 18. Maneuvers in all directions are commanded, which is an indicator of satisfactory guidance since impacts are predicted near the target in all directions. The surveyed impact point on the firing range for this flight was less than 1 m from the intended target.

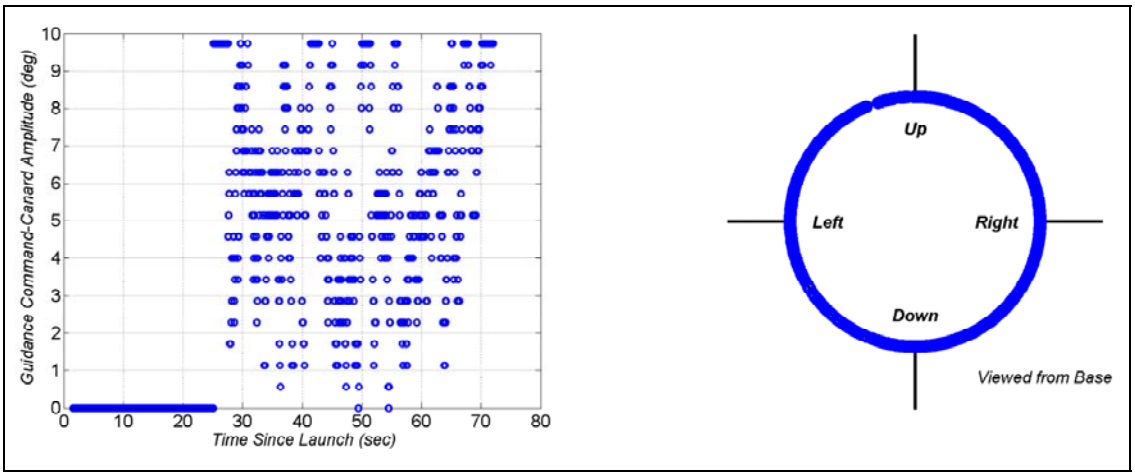

Figure 7. Guidance commands during the flight experiments.

4. Six Degree-of-Freedom Modeling and Monte Carlo System Simulation

Full spectrum performance of this guidance and control scheme, beyond the experimental results, was obtained through modeling and simulation. A 6-DOF model of the system was built. Body-fixed equations of motion for the kinematics and dynamics of the projectile were used (*7*, *8*).

Aerodynamic modeling consisted of terms for the axial force, normal force, pitching moment, pitch damping moment, side moment, static roll moment, and dynamic roll moment as a function of Mach number, angle-of-attack, roll angle, and canard deflection. These aerodynamics were obtained through wind tunnel testing and experimental flights (*25*). Physical properties (e.g., mass, inertia, center-of-gravity) were obtained through solid modeling and measurements.

Various models were included within this simulation architecture to more properly represent physical reality in a stochastic sense. Perturbations to the standard atmosphere were included by introducing meteorological (Met) staleness. This models variation in atmospheric temperature, pressure, and density with altitude as a function of degree of Met staleness (e.g., half-hour, four-hour). Steady wind speed and direction were also included in the simulation via stale Met tables. Additionally, a Dryden wind turbulence model was incorporated.

The GPS model included bias and random error terms for position (three-axis), velocity (three-axis), and roll orientation. A white sequence was assumed for all random errors. The noise density for the position bias error was $\aleph(0,\sigma_{bias}^{position})$ and position random error was $\aleph(0,\sigma_{random}^{position})$. Similarly, the noise distribution for the velocity noise error was $\aleph(0,\sigma_{random}^{velocity})$. GPS should not have a significant velocity bias error provided the space and control error does not vary significantly over the flight and the receiver clock does not drift appreciably. Roll bias error was given by $\aleph(0,\sigma_{bias}^{roll})$ and roll random error was prescribed by $\aleph(0,\sigma_{random}^{roll})$. Laboratory, field, and flight experiments were conducted to obtain realistic values for the GPS errors.

The CAS model included the actual CAS controller used in the system and a dynamic model of the CAS. Monte Carlo simulations were performed with this CAS model enabled and disabled. Both cases showed similar results. The CAS model was not used in the results presented herein since CAS control was so near ideal that adding the addition complexity showed no discernable difference and significantly increased run time.

A Monte Carlo wrapper was built around the simulation to facilitate stochastic analysis. Initial conditions of flight (muzzle velocity, quadrant elevation, gun azimuth, roll rate) and projectile parameters (aerodynamics, physical properties) were perturbed from nominal. Random number seeds ensured simulation repeatability. Impact points were the metric of interest from these simulations which enabled impact statistics to be calculated.

5. Expected Precision

The modeling and simulation environment was exercised to answer the following questions: what is the expected level of precision and how do the navigation and guidance and control uniquely contribute to the overall precision? In this concept, the navigation data (position,

velocity, and roll) are provided by the GPS. Simulations were performed to assess the significance of position-velocity-related errors separate from roll errors. Errors due to the guidance and control algorithm were isolated by subtracting the simulation impact statistics from the navigation errors.

Table 1 provides the cases that were each run for 1000 trials in the 6-DOF/system simulation environment. Nominal quadrant elevation was 50° and muzzle velocity was 696 m/s. Guidance start time was 25 s and the target was placed 16 km from the gun for the guided cases. Characterization of the ballistic dispersion, four levels of position-velocity error, and three levels of roll error were undertaken. The magnitude of position-velocity related errors are defined by a new variable: the standard deviation of the combined position-velocity error (σ_{PV}). Roll errors were separated into low, medium, and high categories. The magnitude of navigation errors (position, velocity, and roll) are simplified and do not represent any realistic tactical scenario. This analysis is only meant to map navigation error to precision and ultimately isolate the error in the guidance and control algorithm.

Table 1. System simulation cases.

Case	$\sigma_{bias}^{position}$ **(m)**	$\sigma_{random}^{position}$ **(m)**	$\sigma_{random}^{velocity}$ **(m/s)**	σ_{bias}^{roll} **(°)**	σ_{random}^{roll} **(°)**
$\sigma_{PV} = 0$, no roll error	0	0	0	0	0
$\sigma_{PV} = 1$, medium roll error	1	1	0.1	5	10
$\sigma_{PV} = 5$, low roll error	5	5	0.5	1	2
$\sigma_{PV} = 5$, medium roll error	5	5	0.5	5	10
$\sigma_{PV} = 5$, medium roll error	5	5	0.5	20	40
$\sigma_{PV} = 10$, high roll error	10	10	1	5	10

Typical impacts from the system simulations are shown in figure 8. The upper portion is the ballistic case. Nominally, the gun azimuth is pointed along the crossrange axis at 0 m. Projectile drift causes the mean point of impact in the crossrange direction to fall past 200 m to the left of the LOF when viewed from behind the gun. More spread in the impacts is apparent in the downrange direction than the crossrange direction due to coupling of the error budget with the flight dynamics and the angle-of-fall obliquity (nominally near 60° from horizontal). Circular error probable (CEP) for the ballistic case is around 200 m.

Impacts for the unrealistic case of no navigation errors are shown in the bottom portion of figure 8. All 1000 impacts fall closer than 1 m to the target point.

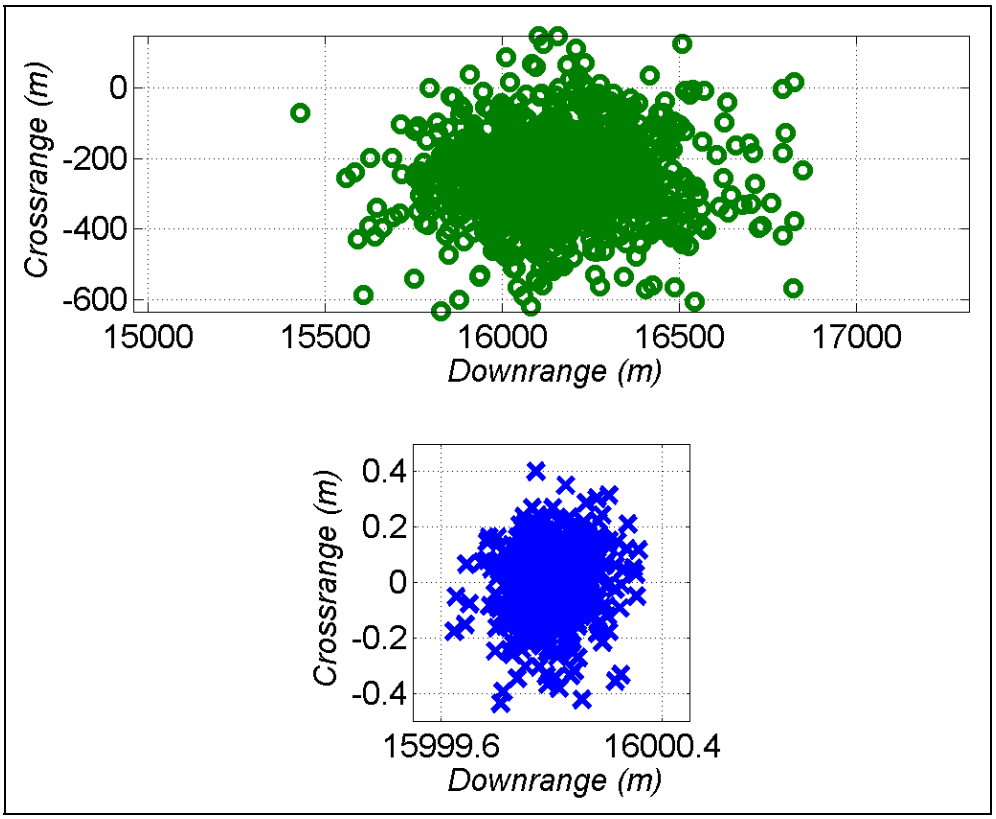

Figure 8. Impacts for ballistic and guided flights with no navigation error from system simulations.

Histograms (of 20 bins each) for some of the cases are given in figure 9. The upper portion of figure 9 is for the ballistic case. The shape of these data suggests a Poisson-like distribution; however, statistical tests for verification have not been performed. Three guided cases (σ_{PV} = 1, 5, 10) with medium roll error are presented at the bottom of figure 9. A cursory examination of these data indicates a CEP around 1, 5, and 10 m for the σ_{PV} = 1, σ_{PV} = 5, and σ_{PV} = 10 cases, respectively.

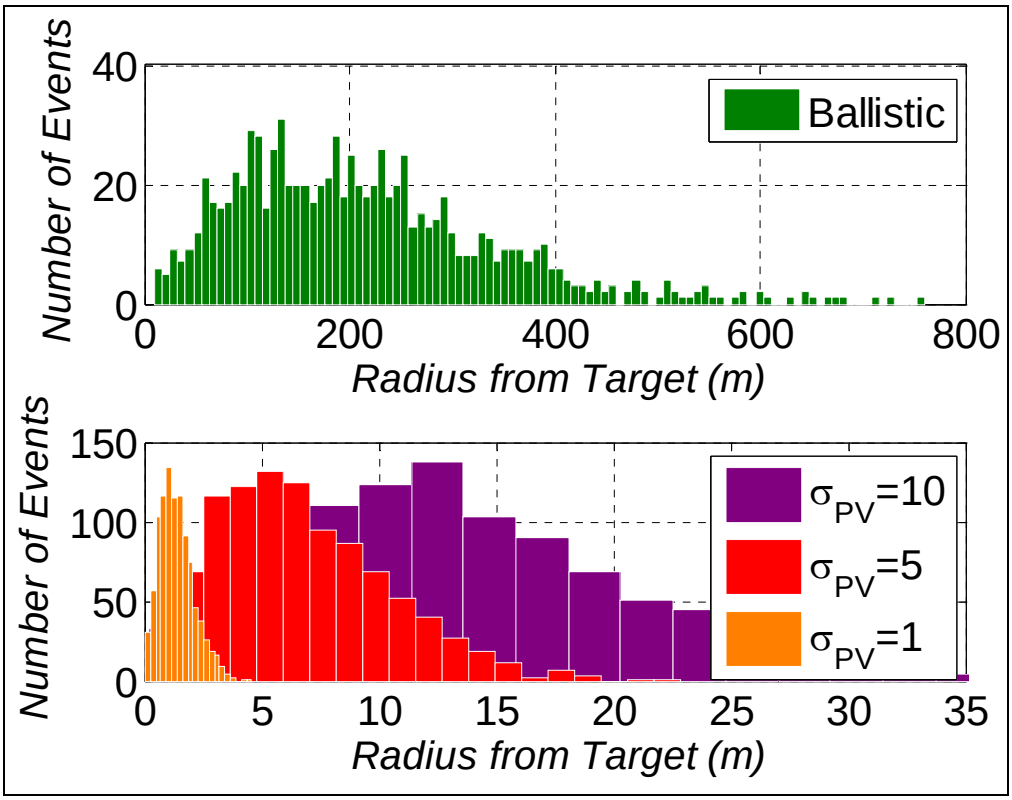

Figure 9. Histograms for ballistic and guided flights with different levels of position-velocity errors and medium roll error from system simulations.

The standard deviation of impacts in the downrange and crossrange directions was calculated for each case. The downrange standard deviation was mapped into the plane normal to impact to remove the effect of impact obliquity. These downrange and crossrange metrics were averaged since they were very close in magnitude to produce the impact standard deviation (σ_{impact}) in figure 10a. Results in figure 10a indicate a linear relationship of precision with position-velocity error. The magnitude of the position bias in the plane perpendicular to impact likely drives the precision.

Guidance and control standard deviation (σ_{GC}) was estimated by subtracting σ_{impact} from σ_{PV} since navigation and guidance and control are the only means to remove errors in the simulation. Here, statistical independence of navigation and guidance and control errors are assumed. Results in figure 10b suggest that $\sigma_{GC} \sim 0.1$ m for all cases but $\sigma_{PV} = 10$ m. Perhaps navigation and guidance and control errors are dependent or enough trials have not been performed to assess such small changes in magnitude. Regardless, the modeling and simulation efforts indicate errors due to the guidance and control algorithm are small compared to the navigation error.

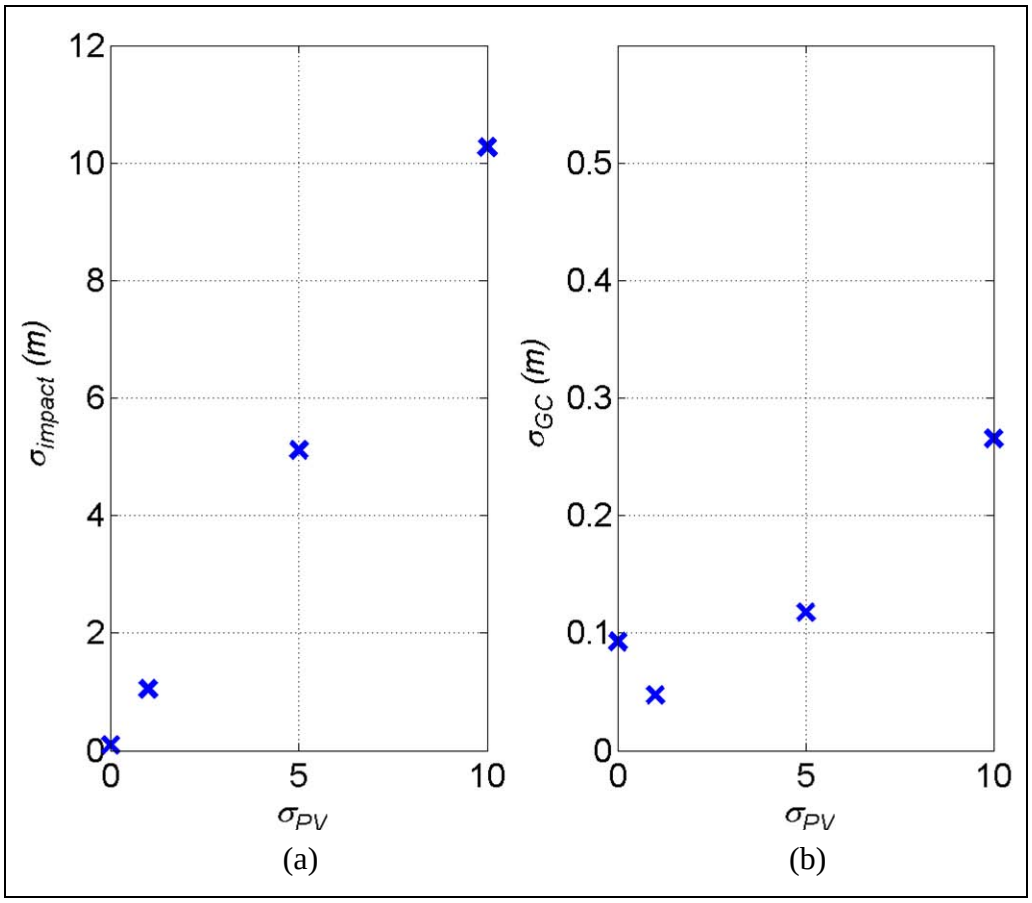

Figure 10. Statistics for total impact error (a) and guidance and control impact error (b) with different levels of position and velocity errors from system simulations.

Figure 11 presents the effect of roll error on precision. Negligible differences in precision with the low, medium, and high roll errors show that the system is quite tolerant to error in roll. The airframe is rolling and actuating with a sinusoid; therefore, relatively large components of maneuver in an undesirable direction still provide a sufficient component of maneuver in the desired direction.

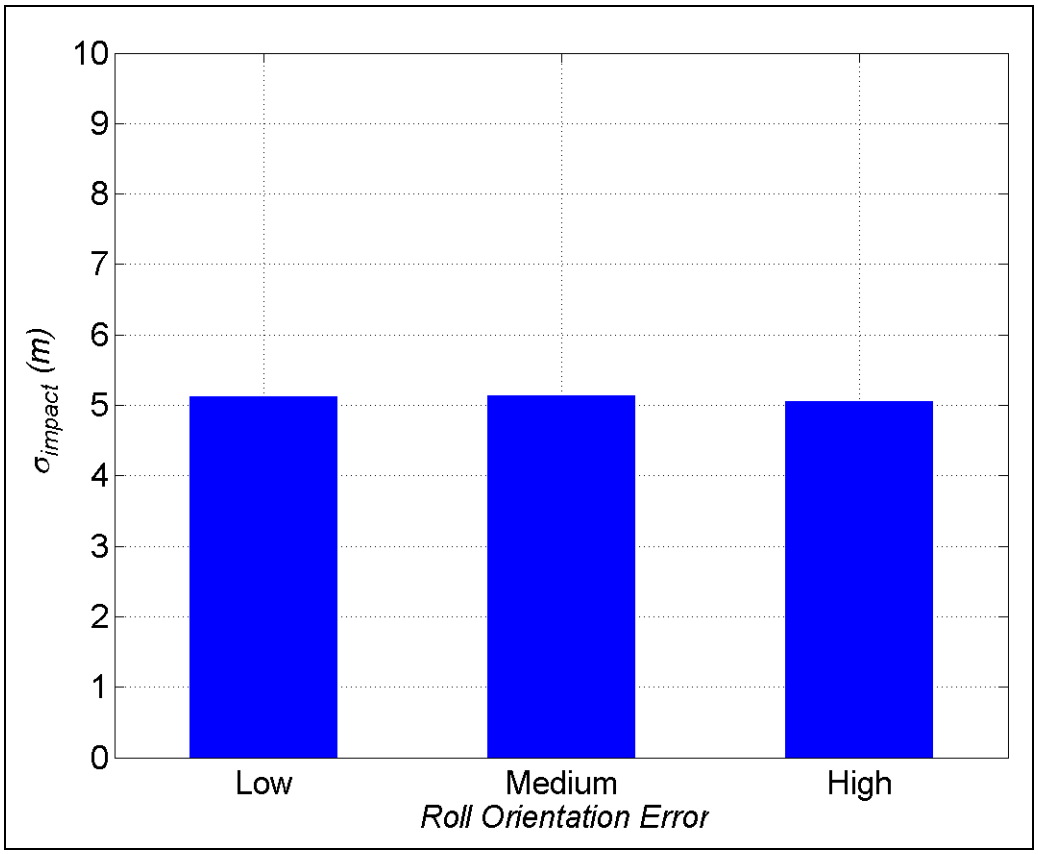

Figure 11. Statistics for total impact error with different levels of roll error from system simulations.

6. Reduced Control Effort

The optimality of this guidance and control approach for control authority-limited airframes is important to highlight. Often, constraints such as affordability, narrowed design space, and packaging limit the control authority for gun-launched applications. This situation occurred for a guided mortar program. The guidance and control algorithm of this effort was applied to this low control authority airframe. As a result, the most sparing maneuvers required to still enable successful guide-to-hit flight experiments were commanded.

Modeling and simulations were performed to illustrate the maneuver conservation aspect of this algorithm. A 6-DOF simulation of the mortar was built with aerodynamics obtained from wind tunnel, computational fluid dynamics (CFD), and flight experiments (*25*). Two flights were simulated: one in which a maximum maneuver was performed throughout flight and one in which the guidance and control algorithm of this effort was used to guide to the target. Guidance started at 15 s for these simulated flights.

The lateral acceleration capability, measured in G's, was obtained from the maximum maneuver flight. The lateral acceleration commanded by the guidance and control algorithm of this effort was calculated from the guided flight. The projectile state data from the 6-DOF for the guided flight was used to compute the traditional proportional navigation lateral acceleration commands. This allows the lateral acceleration from the algorithm developed in this effort to be directly compared with proportional navigation requirements.

Figure 12 shows the lateral acceleration available from this mortar airframe. Maneuverability is extremely low, less than a tenth of a G, and varies mainly with dynamic pressure. The lateral acceleration pulled by the impact point prediction algorithm to hit the target point is less than the available G's. Acceleration commands from the proportional navigation guidance law, however, are about an order of magnitude higher than the available G's throughout the flight. Proportional navigation attempts to prescribe engagement geometry for intercept which either spends all maneuverability early in flight or over-controls the airframe and correspondingly the target point cannot be hit. This underscores the importance in including the flight dynamics in the guidance and control algorithm for control authority-limited projectiles.

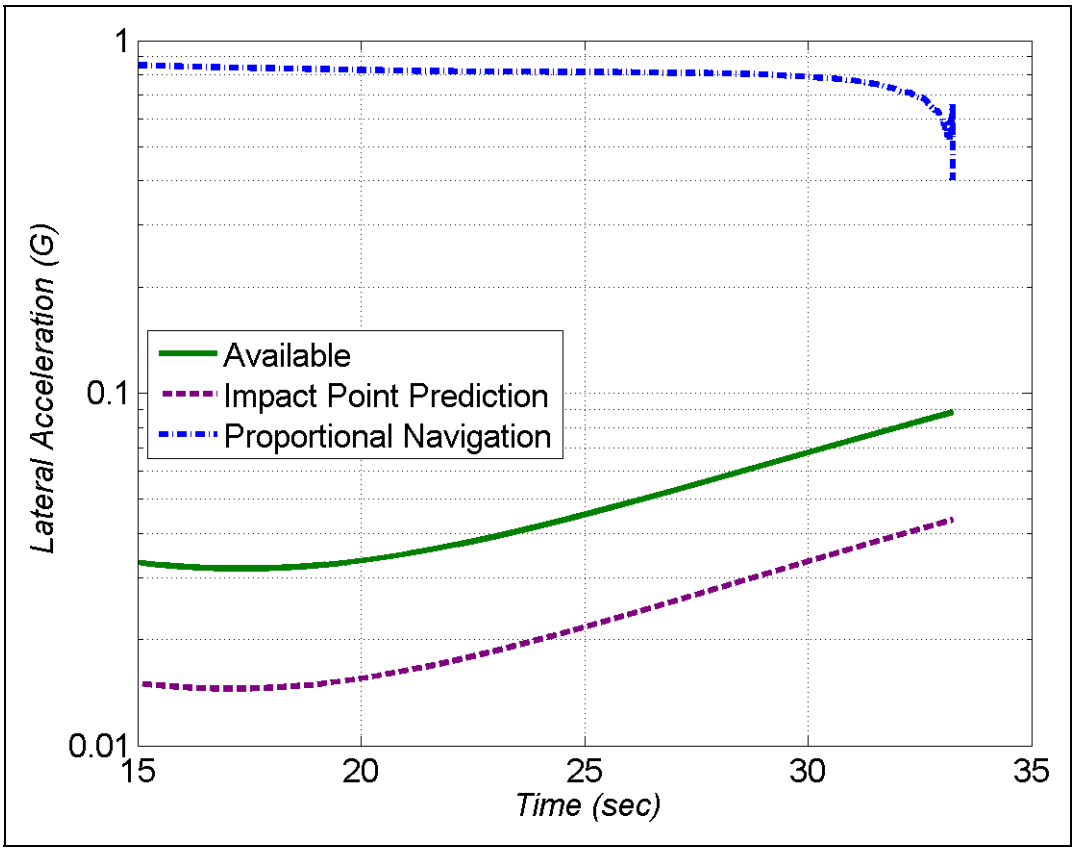

Figure 12. Lateral acceleration capability of reduced actuator requirement airframe and commands from impact point prediction and proportional navigation guidance.

7. Rapid Scalability to Other Calibers

As intimated previously, the guidance and control algorithm was also used for flight experiments of an entirely different system. A short timeframe was available between flight experiments of a 120-mm airframe and the 155-mm projectile described previously. Successful guide-to-hit flights were enabled on both calibers by this algorithm due to factors such as the minimal aerodynamic characterization and algorithm tuning required.

The guidance and control algorithm was updated with the physical properties and aerodynamics of the 120-mm mortar. A process similar to that outlined above for the 155-mm projectile was undertaken to prepare for gun firings. Comparable GPS, CAS, and diagnostic hardware were used for the experiments.

Gun firings were performed at the Aberdeen Proving Ground, MD, with similar instrumentation. Mortars were launched at about a 62° quadrant elevation and a 233-m/s muzzle velocity. The target was located 3800 m from the gun. The guidance start time was 13 s and the ECEF coordinates of the gun and target were loaded into the algorithm before firing.

An example of the algorithm performance in flight for the 120-mm mortar, obtained through the telemetry stream, is provided in figure 13. These data show the position error, which is the difference between the impact point prediction and the target point in the downrange (X) and crossrange (Y) directions. Trends in this data follow those described for the impact point predictions of the 155-mm projectile. Position error fluctuates before converging to zero near impact. The surveyed impact of this shot was less than 10 m from the target point.

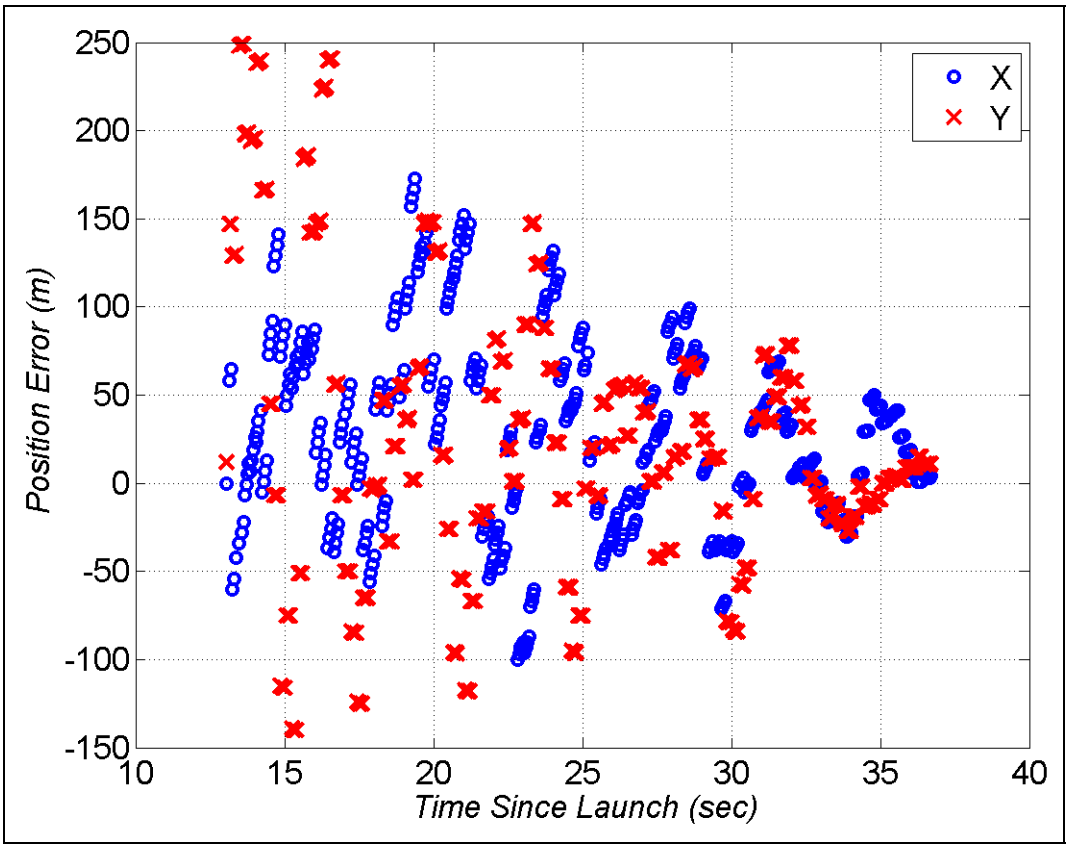

Figure 13. Downrange and crossrange impact point prediction-to-target point error during flight experiments of mortar.

8. Trajectory Shaping

This guidance and control approach is flexible when sufficient control authority is available to enable trajectory shaping. The important point is that the guidance and control must be developed alongside the airframe to ensure that the commanded maneuvers are actually realizable in flight.

The 6-DOF simulation of the 155-mm artillery projectile was used to demonstrate the trajectory shaping feature of this algorithm. The center-of-gravity of this projectile was shifted toward the base slightly in simulation to increase control authority. Two guided flights with different values of the trajectory shaping parameter $\bar{\alpha}$ were executed in the 6-DOF simulation. The target was placed 16 km from the gun and guidance began at 25 s.

Altitude and angle-of-attack variation with downrange distance from the simulation for the two nominal and shaped cases are presented in figure 14. The nominal trajectory reaches about 6.5 km in altitude, but the shaped trajectory goes almost to 7 km. Impact angle was steepened by almost 20°, from 66–84°, due to this maneuver.

Angle-of-attack history provides further understanding of how this trajectory shaping takes place. The nominal flight skipped through the glide phase and performed a small pitch-over maneuver (negative angle-of-attack) when entering the endgame phase. Angle-of-attack was near zero as the projectile was on a ballistic-based collision course with the target point.

A different angle-of-attack response was attained for the trajectory shaping flight. As the trajectory shaping parameter was increased the guidance remains in the glide phase for a much longer duration (from about 8000 m to 14,000 m downrange). The glide angle-of-attack varied from near 5° to 10° due to changes in flight conditions. At transition to endgame, a pitch-over maneuver occurs for about 2 km of downrange distance because the airframe needs to pull down after gliding so near the target. Angle-of-attack is near zero for the final seconds of flight.

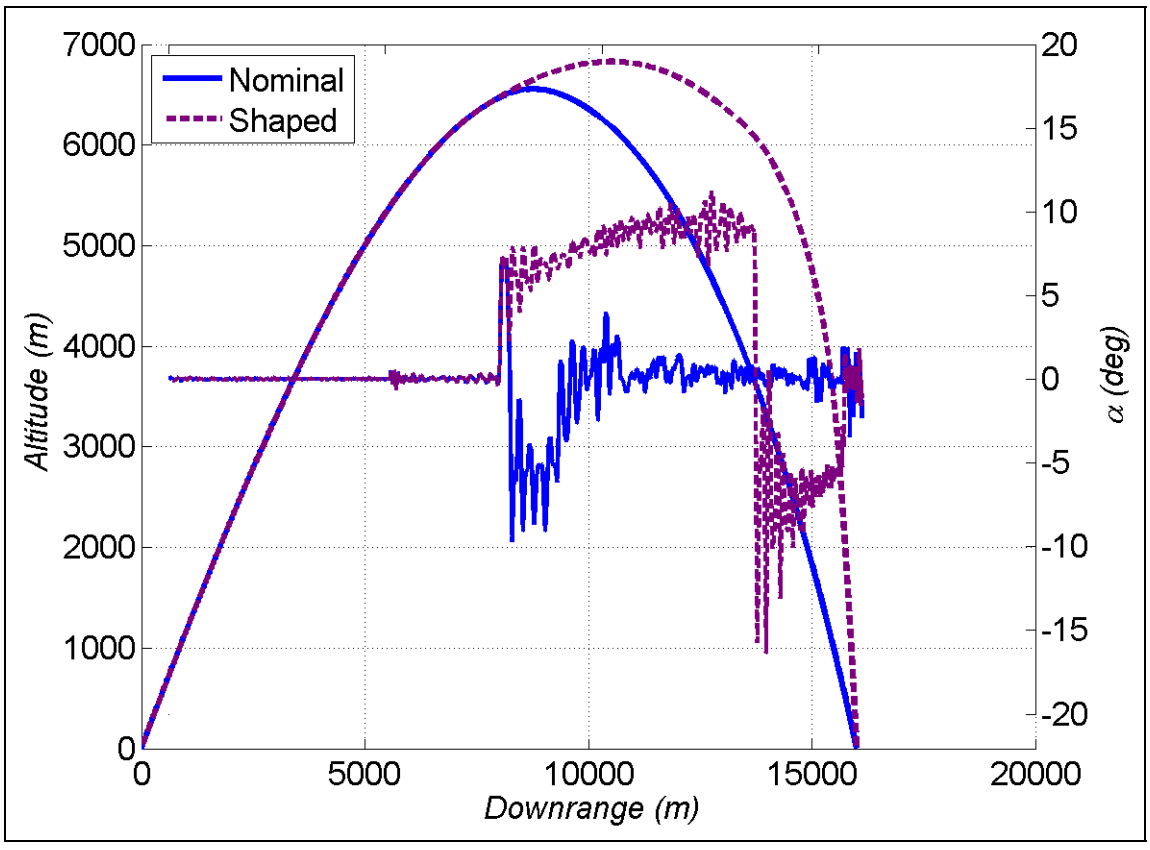

Figure 14. Trajectory and angle-of-attack history for nominal and trajectory shaping guidance.

9. Conclusions

A novel guidance and control approach for precision munitions was developed in this effort. Embedding the nonlinear flight dynamics into the guidance and control provided immense capability. Requirements for sensors and actuators are reduced. Precision was driven by the position bias error; the system was intolerant of errors in velocity and roll. Impact errors due to the guidance and control were near 0.1 m. Maneuvers were conserved, which is especially important for control authority-limited airframes. Embedded processing was optimal since a closed-form solution to the flight dynamic model was obtained. Importantly, the projectile states required for the flight dynamic model were obtained from affordable, available sensors. The generality of the algorithm permits rapid application to different airframes. Lastly, trajectory shaping was enabled through this guidance and control approach. The airframe must be developed in tandem with the guidance and control algorithm, however, to fully exploit the maneuverability available. These features of the algorithm were verified and demonstrated through state-of-the-art flight experiments and modeling and simulation.

10. References

1. Morrison, P. H.; Amberntson, D. S. Guidance and Control of a Cannon-Launched Guided Projectile. *J of Spacecraft and Rockets* **1977**, *14* (6), 328–334.
2. Grubb, N. D.; Belcher, M. W. Excalibur: New Precision Engagement Asset in the Warfight. *Fires* **2008**, 14–15.
3. Davis, B.; Malejko, G.; Dorhn, R.; Owens, S.; Harkins, T.; Bischer, G. Addressing the Challenges of a Thruster-Based Precision Guided Mortar Munition With the Use of Embedded Telemetry Instrumentation. *ITEA Journal* **2009**, *30*, 117–125.
4. Moorhead, J. S. Precision Guidance Kits (PGKs): Improving the Accuracy of Conventional Cannon Rounds. *Field Artillery* **2007**, 31–33.
5. Ollerenshaw, D.; Costello, M. Simplified Projectile Swerve Solution for General Control Inputs. *J. of Guidance, Control, and Dynamics* **2008**, *31* (5), 1259–1265.
6. Fresconi, F.; Plostins, P. Control Mechanism Strategies for Spin-Stabilized Projectiles. *J. of Aerospace Engineering* **2010**, *224* (G9), 979–992.
7. Nicolaides, J. *On Missile Flight Dynamics*; Catholic University of America, Ph.D dissertation, 1963.
8. Murphy, C. *Free Flight of Symmetric Missiles*; BRL-Report Number-1216; U.S. Army Ballistics Research Laboratory: Aberdeen Proving Ground, MD, 1963.
9. Cooper, G.; Costello, M.; Fresconi, F.; DeSpirito, J.; Celmins, I. *Flight Stability of Asymmetric Projectiles with Control Mechanisms*; AIAA, Paper No. 2010–7636, August 2010.
10. Calise, A. J.; Sharma, M.; Corban, J. E. Adaptive Autopilot Design for Guided Munitions. *J. of Guidance, Control, and Dynamics* **2000**, *23* (5), 837–843.
11. Jitpraphai, T.; Costello, M. Dispersion Reduction of a Direct Fire Rocket Using Lateral Pulse Jets. *J. of Spacecraft and Rockets* **2001**, *38* (6), 929–936.
12. Rogers, J.; Costello, M. Design of a Roll-Stabilized Mortar Projectile with Reciprocating Canards. *J. of Guidance, Control, and Dynamics* **2010**, *33* (4), 1026–1034.
13. Calise, A. J.; El-Shirbiny, H. A. An Analysis of Aerodynamic Control for Direct Fire Spinning Projectiles. *Guidance, Navigation and Control Conference*, AIAA 2001-4217, August 2001.

14. Burchett, B.; Costello, M. Model Predictive Lateral Pulse Jet Control of an Atmospheric Rocket. *J. of Guidance, Control, and Dynamics* **2002**, *25* (5), 860–867.

15. Ollerenshaw, D.; Costello, M. Model Predictive Control of a Direct Fire Projectile Equipped with Canards. *J. of Dynamic Systems, Measurement, and Control* **2008**, *130.*

16. Pamadi, K. B.; Ohlmeyer, E. J.; Pepitone, T. R. Assessment of a GPS Guided Spinning Projectile Using an Accelerometer-Only IMU. *Guidance, Navigation and Control Conference*, AIAA 2004-4881, August 2004.

17. Pamadi, K. B.; Ohlmeyer, E. J. Evaluation of Two Guidance Laws for Controlling the Impact Flight Path Angle of a Naval Gun Launched Spinning Projectile. *Guidance, Navigation and Control Conference,* AIAA 2006-6081, August 2006.

18. Slegers, N. Predictive Control of a Munition Using Low-Speed Linear Theory. *J. of Guidance, Control, and Dynamics* **2008**, *31* (3), 768–775.

19. Hahn, P. V.; Frederick, R. A.; Slegers, N. Predictive Guidance of a Projectile for Hit-to-Kill Interception. *IEEE Transactions on Control Systems Technology* **2009**, *17* (4), 745–755.

20. Phillips, C. A. Guidance Algorithm for Range Maximization and Time-of-Flight Control of a Guided Projectile. *J. of Guidance, Control, and Dynamics* **2008**, *31* (5), 1447–1455.

21. Chandgadkar, S.; Costello, M.; Dano, B.; Liburdy, J.; Pence, D. Performance of a Smart Direct Fire Projectile Using Ram Air Control Mechanism. *J. of Dynamic Systems, Measurement, and Control* **2002**, *124*, 606–612.

22. Fresconi, F.; Brown, T.; Celmins, I.; DeSpirito, J.; Ilg, M.; Maley, J.; Magnotti, P.; Scanlan, A.; Stout, C.; Vazquez, E. Very Affordable Precision Projectile System and Flight Experiments. *27th Army Science Conference*, Orlando, FL, 2010.

23. Fresconi, F.; Cooper, G.; Costello, M. Practical Assessment of Real-Time Impact Point Estimators for Smart Weapons. *J. of Aerospace Engineering* **2011**, *24* (1).

24. Fresconi, F. Range Extension of Gun-Launched Smart Munitions, *International Ballistics Symposium*, Paper No. 113, 2008.

25. Fresconi, F.; Harkins, T. Aerodynamic Characterizations of Asymmetric and Maneuvering 105mm, 120mm, and 155mm Fin-Stabilized Projectiles Derived from Telemetry Experiments. manuscript in preparation.

List of Symbols, Abbreviations, and Acronyms

6-DOF	six degree-of-freedom
CAS	control actuation system
CEP	circular error probable
CFD	computational fluid dynamics
DSP	digital signal processor
ECEF	Earth-centered, Earth-fixed
GNC	guidance, navigation, and control
GPS	global positioning system
GTL	gun-target line
LOF	line-of-fire

NO. OF
COPIES ORGANIZATION

1 (PDF only) DEFENSE TECHNICAL INFORMATION CTR
DTIC OCA
8725 JOHN J KINGMAN RD
STE 0944
FORT BELVOIR VA 22060-6218

1 DIRECTOR
US ARMY RESEARCH LAB
IMNE ALC HRR
2800 POWDER MILL RD
ADELPHI MD 20783-1197

1 DIRECTOR
US ARMY RESEARCH LAB
RDRL CIM L
2800 POWDER MILL RD
ADELPHI MD 20783-1197

1 DIRECTOR
US ARMY RESEARCH LAB
RDRL CIM P
2800 POWDER MILL RD
ADELPHI MD 20783-1197

1 DIRECTOR
US ARMY RESEARCH LAB
RDRL D
2800 POWDER MILL RD
ADELPHI MD 20783-1197

ABERDEEN PROVING GROUND

1 DIR USARL
RDRL CIM G (BLDG 4600)

NO. OF COPIES	ORGANIZATION
6	RDECOM ARDEC RDAR MEF E D CARLUCCI M HOLLIS C STOUT A SANCHEZ R HOOKE J MURNANE BLDG 94 PICATINNY ARSENAL NJ 07806-5000
8	RDECOM ARDEC RDAR MEF S D PANHORST G MINER N GRAY R FULLERTON B DEFRANCO M MARSH P FERLAZZO D PASCUA BLDG 94 PICATINNY ARSENAL NJ 07806-5000
4	RDECOM ARDEC RDAR MEM C D NGUYEN R GORMAN D CIMORELLI K SANTANGELO BLDG 94 PICATINNY ARSENAL NJ 07806-5000
3	RDECOM ARDEC D DEMELLA P MAGNOTTI A LICHTENBERG-SCANLAN BLDG 61S PICATINNY ARSENAL NJ 07806-5000
2	RDECOM ARDEC RDAR MEM M C MOEHRINGER J TRAVAILLE BLDG 94 PICATINNY ARSENAL NJ 07806-5000
4	RDECOM ARDEC RDAR MEM A E VAZQUEZ T RECCHIA G MALEJKO W KOENIG BLDG 94S PICATINNY ARSENAL NJ 07806-5000
3	RDECOM ARDEC J GRAU W TOLEDO S CHUNG BLDG 95 PICATINNY ARSENAL NJ 07806-5000
3	RDECOM ARDEC RDAR MEF I R GRANITZKI J CHOI L VO BLDG 95 PICATINNY ARSENAL NJ 07806
1	RDECOM ARDEC RDAR MEM C M LUCIANO BLDG 65S PICATINNY ARSENAL NJ 07806
1	US ARMY ARDEC PROPULSION INDIRECT FIRE BR RDAR MEE W J LONGCORE BLDG 382 PICATINNY ARSENAL NJ 07806
1	RDECOM ARDEC RDAR MEF M HOHIL BLDG 407 PICATINNY ARSENAL NJ 07806-5000

NO. OF COPIES ORGANIZATION

4 RDECOM ARDEC
AMSRD AMR SG SD
J BAUMAN
H SAGE
S DUNBAR
B NOURSE
BLDG 5400
REDSTONE ARSENAL AL 35898

2 PM CAS
SFAE AMO CAS
R KIEBLER
P MANZ
BLDG 171
PICATINNY ARSENAL NJ 07806

2 PM CAS
SFAE AMO CAS EX
J MINUS
M BURKE
BLDG 171
PICATINNY ARSENAL NJ 07806

3 PM MORTAR SYS
SFAE AMO CAS MS
P BURKE
G SCHWARTZ
J HILT
BLDG 162S
PICATINNY ARSENAL NJ 07806-5000

1 PM MAS
SFAE AMO MAS
C GRASSANO
BLDG 354
PICATINNY ARSENAL NJ 07806

1 PM MAS
SFAE AMO MAS LC
D RIGOGLIOSO
BLDG 354
PICATINNY ARSENAL NJ 07806

1 PM MAS
SFAE AMO MAS SETI
J FOULTZ
BLDG 354
PICATINNY ARSENAL NJ 07806

NO. OF COPIES ORGANIZATION

1 FIRES DEPUTY MGR
EXP MANEUVER WARFARE
OFC OF NAVAL RSRCH
ONR 30
875 NORTH RANDOLPH ST
RM 1155B
ARLINGTON VA 22203

2 NAVAL SURFACE WARFARE CTR
DAHLGREN DIVISION
N COOK
L STEELMAN
G33
6210 TISDALE RD STE 223
DAHLGREN VA 22448-5114

1 ALLIANT TECHSYSTEMS INC
ALLEGANY BALLISTICS LAB
S OWENS
MS WV01 08 BLDG 300 RM 180
210 STATE RTE 956
ROCKET CTR WV 26726-3548

1 SAIC
J NORTHRUP
8500 NORMANDALE LAKE BLVD
STE 1610
BLOOMINGTON MN 55437-3828

1 SAIC
D HALL
1150 FIRST AVE STE 400
KING OF PRUSSIA PA 19406

1 GEN DYNAMICS ST MARKS
H RAINES
PO BOX 222
SAINT MARKS FL 32355-0222

1 GEN DYNAMICS ARM SYS
J TALLEY
128 LAKESIDE AVE
BURLINGTON VT 05401

4 BAE ARM SYS DIV
T MELODY
J DYVIK
P JANKE
B GOODELL
4800 E RIVER RD
MINNEAPOLIS MN 55421-1498

NO. OF
COPIES ORGANIZATION

1 US ARMY YUMA PROVING GROUND
TEDT YPY MW
M BARRON
301 C STREET
YUMA AZ 85365-9498

1 TRAX INTRNTL CORP
R GIVEN
US ARMY YUMA PROVING GROUND
BLDG 2333
YUMA AZ 85365

1 ARROW TECH ASSOC
W HATHAWAY
1233 SHELBURNE RD
STE D-8
SOUTH BULINGTON VT 05403

1 GEORGIA INST OF TECHLGY
SCHOOL OF AEROSPACE ENG
M COSTELLO
ATLANTA GA 30332

ABERDEEN PROVING GROUND

6 COMMANDER
US ARMY TACOM ARDEC
AMSRD AR AEF D
R LIESKE
J MATTS
A SOWA
J FONNER
M ANDRIOLO
B NARIZZANO

47 DIR USARL
RDRL WM
P PLOSTINS
RDRL WML
M ZOLTOSKI
J NEWILL
RDRL WML A
W OBERLE
R PEARSON
L STROHM
RDRL WML D
J SCHMIDT
M NUSCA
RDRL WML E
I CELMINS
G COOPER
J DESPIRITO
L FAIRFAX

NO. OF
COPIES ORGANIZATION

F FRESCONI (5 CPS)
J GARNER
B GUIDOS
B HOWELL
G OBERLIN
J SAHU
S SILTON
P WEINACHT
RDRL WML F
F BRANDON
T BROWN
B DAVIS
T HARKINS
D HEPNER
M ILG
G KATULKA
D LYON
J MALEY
R MCGEE
C MILLER
P MULLER
P PEREGINO
D PETRICK
B TOPPER
RDRL WML G
W DRYSDALE
M MINNICINO
J BENDER
RDRL WML H
C CANDLAND
M FERMER-COKER
R SUMMERS
RDRL WMP F
N GNIAZDOWSKI
R BITTING

INTENTIONALLY LEFT BLANK.